Received: 9 June 2022 | Revised: 5 December 2022 | Accepted: 13 December 2022

DOI: 10.1002/asna.20220042

Astronomische Nachrichten

ORIGINAL ARTICLE

Multifractal cross-correlation analysis between CME and Planetary K-index time series

Anirban Chattopadhyay | **Mofazzal H. Khondekar**

Electronics and Communication Engineering, Dr. B.C. Roy Engineering College, Durgapur, India

Correspondence
Anirban Chattopadhyay, Electronics and Communication Engineering,
Dr. B.C. Roy Engineering College,
Durgapur, India.
Email: chatterjee.anirban7@gmail.com

Abstract

This research aims to examine the multiscale-multifractal correlation properties between the geomagnetic storm and coronal mass ejection (CME) occurrences by analyzing the CME linear speed and Planetary K-index time series data. The relevant data for both CME and geomagnetic storm occurrences were obtained from the Solar and Heliospheric Observatory mission's LASCO and the NOAA Space Weather Prediction Center, respectively, for the same period (February 1999 to December 2007). We performed MultiFractal cross-correlation Detrended Fluctuation Analysis (MFXDFA) and Multifractal cross-correlation Detrending Moving average Analysis (MFXDMA) to investigate and quantify the possible cross-correlation between the two natural events. The MFXDFA technique is also compared to the backward MFXDMA algorithm's performance. The change in the degree of cross-correlation over time has been investigated, and the findings are quantitatively analyzed. The existence of significant power-law cross-correlations has been discovered within all scaling orders. Furthermore, we also find evident persistence of cross-correlation with substantial Hurst exponents. In addition, it has been observed that long-term cross-correlation has a more considerable degree of multifractality and persistence than short-term cross-correlation.

KEYWORDS

coronal mass ejection, multifractal cross-correlation detrended fluctuation analysis, multifractal cross-correlation detrending moving average analysis, Planetary K-index

1 | INTRODUCTION

The Earth's magnetic field might be considered as our planet's only defense against the Sun's high-energy particles and hazardous radiation. According to the scientific community, significant changes in the geomagnetic field generated by different solar activities may jeopardize the operation of crucial infrastructures relying on space-based assets and have terrestrial effects. The fundamental mechanics, on the other hand, are still not clear. By analyzing CME linear speed and Planetary K-index (Kp-index) data, an attempt has been made to explore the cross-correlations between the Coronal Mass Ejection (CME) and the occurrence of geomagnetic storms. Coronal Mass Ejection (CME) is a sort of severe solar event that occurs when a massive cloud of magnetically charged plasma is released from the Sun's corona and travels at large speeds(thousands of kilometers per second) into

interplanetary space. When a CME collides with our planet's atmosphere, it releases large quantities of energy into the magnetosphere, causing massive disruption in the geomagnetic field and triggering a geomagnetic storm. An intense geomagnetic storm poses a massive threat to our civilization of its impact on critical infrastructures such as electrical power, satellite-enabled communications, navigation, and monitoring (Hapgood 2012; Kappenman 1996; Kappenman 2012; Thomson et al. 2010). The intensity of geomagnetic storms may be classified and measured using the Planetary K-index (Kp-index), which is based on a worldwide average of aberrant geomagnetic field changes (Menvielle & Berthelier 1991). NOAA Space Weather Prediction Center (SWPC) derives the estimated 3-hour Planetary K-index using the data from ground-based magnetometers located in different countries. The Kp- index varies from 0 to 9, with a value greater than or equal to 5 suggesting an extreme geomagnetic storm.

The Solar and Heliospheric Observatory (SOHO) obtained the CME time series data from February 1999 to December 2007 as summarized in the CME catalogue[1] (Gopalswamy et al. 2009). In their research, Gopalswamy et al. identified four primary attributes of a CME: "linear speed", "width", "CPA", and "acceleration". Here, the 'linear speed' attribute has been chosen as the most appropriate attribute in comparison to the other three parameters (width, CPA, acceleration) for the analysis (Chattopadhyay et al., Stationarity and periodicities of linear speed of coronal mass ejection: a statistical signal processing approach Chattopadhyay et al. 2017). Similarly, the Kp- index data are chosen for the same period (February 1999 to December 2007) from the NOAA Space Weather Prediction Center by determining the average value of the eight 3-hour Kp indices per day for the analysis.[2] An effort has been made here to investigate the cross-correlation between two natural occurrences, namely geomagnetic storm and coronal mass ejection, by analyzing the Kp- index and CME speed signal (see Figure 1).

There have been a large number of geomagnetic storm occurrences reported during solar cycle 23, but only a handful of them have influenced the Earth's environment. Intense geomagnetic storms were observed on October 4–7, 2000, which substantially influenced the ionosphere. Although the ion temperatures of the terrestrial magneto-tail generally used to remain consistent, it has been noticed that in October 2000, the measured ion temperature was 2–3 times more than the average value (Keesee et al. 2008). Another geomagnetic storm event was noticed on October 21, 2001, and its effect has been explained in Jordanova et al. research paper (Jordanova et al. 2008). They have observed the massive loss of electrons in the radiation belt into the atmosphere, and electron flux drops out due to the outward radial diffusion. In October 2003, various intense geomagnetic storm events were registered. As an effect of these geomagnetic storm events, different incidents have been recorded by multiple researchers like increased photoionization effects in the dayside ionosphere (Villante and Regi 2008), enormous ionospheric disturbances which had yielded a "swirling" effect in a direction opposite to the Earth's rotation (Gopalswamy 2009) and high-value GIC (geomagnetically induced currents) which is always a threat to our power grids (Ni 2017). During August–September 2005, various high-value Kp index peaks were noticed, while among them, 24 August, 31 August, 11 September, and 13 September most intense geomagnetic storm events were recorded with a peak Kp index value of ≈ 8 (Papaioannou et al. 2009). The geomagnetic storm events were recorded on 14–15 December 2006 when Earth's magnetosphere was affected by the CME-associated interplanetary shock. Ionospheric disturbances have been recorded due to these geomagnetic storm events which produce increases and decreases in electron densities and total electron content (TEC) and also provide GIC (Sahai et al. 2012; Suvorova et al. 2015; Zhao et al. 2008). In space research, Earth's magnetosphere is always an exciting domain for researchers to explore (Echer et al. 2006; Horvath & Lovell 2017; Holappa et al. 2014; Huttunen et al. 2008; Mansilla 2013).

The scatter plot in Figure 2 reveals a slight positive correlation between the CME Linear speed and the Kp index value. The Pearson Correlation Coefficient is found to be 0.3743, which indicates the degree of the linear relationship between the two. The slope of the Linear regression line that fits the relationship between the CME Linear speed and the Kp index value is 0.57, which corresponds to the angle of 30^0.

The long-term power-law cross-correlations between these two signals have also been verified using the Multifractal cross-correlation detrended fluctuation analysis (MF-X-DFA) algorithm (Zhou 2008). Continuous wavelet transform (CWT) based Semblance Analysis has also been performed to reveal the local phase relationship between two signals (Cooper & Cowan 2008).

The rest of this work is planned as follows. Section 2 summarizes the formal description of the algorithms for MFXDFA and MFXDMA techniques. Section 3 includes different plots of our results along with a detailed discussion on the crucial observations, while the paper concludes in Section 4 with a summary of the results.

[1] http://cdaw.gsfc.nasa.gov/CME_list/index.html.
[2] https://www.swpc.noaa.gov/products/planetary-k-index.

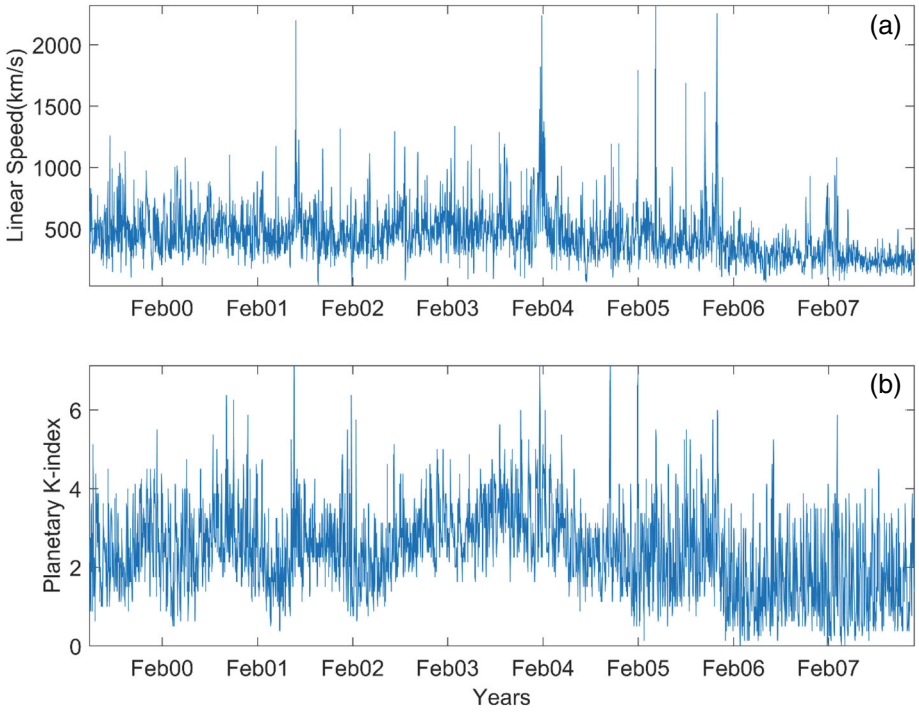

FIGURE 1 Two time series signals from Feb. 1999 to Dec. 2007 (a) CME linear speed signal from SOHO; (b) Kp- index signal from the NOAA—SWPC

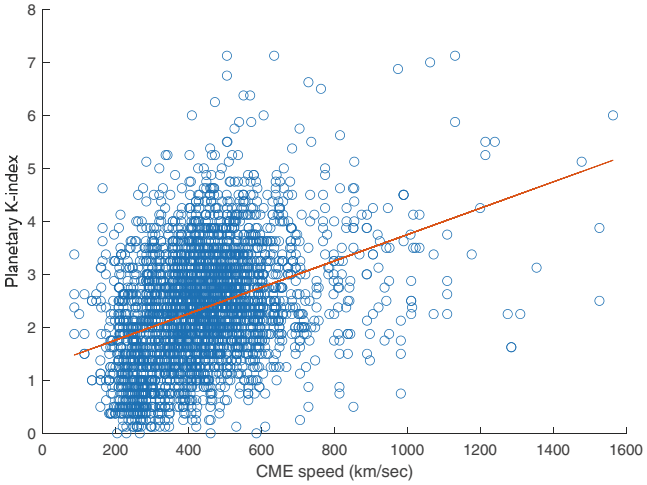

FIGURE 2 Scatter Plot and Linear Regression line for CME Linear speed and Planetary K-Index

2 | ALGORITHMS FOR ANALYSIS

2.1 | Multifractal cross-correlation detrended fluctuation analysis (MFXDFA)

Assuming $\{r_i\}$ and $\{s_i\}$ as two time series of length L, where $i = 1, \cdots, L$ MFXDFA algorithm is summarized as follows based on MFDFA algorithm (Zhou 2008) (Chattopadhyay et al., Fractality and singularity in CME linear speed signal: Cycle 23 Chattopadhyay et al. 2018):

- Step 1: Determine the signal profile of the time series,

$$R(i) = \sum_{n=1}^{i} (r(n) - \bar{r}); \quad i = 1, \cdots, L \tag{1}$$

$$S(i) = \sum_{n=1}^{i} (s(n) - \bar{s}); \quad i = 1, \cdots, L \tag{2}$$

  where $\bar{r}$ and $\bar{s}$ are the sample averages.
- Step 2: Profile $R(i)$ and $S(i)$ are split into L_s number of non-overlapping segments of length s, where $L_s = \text{int}(L/S)$. Usually, a short tail always remains at the signal profile because mostly the data length L is not a multiple of time scale s. Hence, the same process is repeated again but from the opposite end this time to incorporate this profile tail. Therefore, $2L_s$ segments are obtained altogether.
- Step 3: The variance $F^2(s, m)$ has been computed by determining the local trends for each segment m using the least square fit method.

$$F^2(s, m) = \frac{1}{s} \sum_{i=1}^{s} \left| R((m-1)s + i) - \widetilde{R}_m(i) \right| \times \left| S((m-1)s + i) - \widetilde{S}_m(i) \right|; \quad m = 1, \cdots, L_s \tag{3}$$

$$F^2(s,m) = \frac{1}{s}\sum_{i=1}^{s}\left|R\left(L-(m-L_s)\,s+i\right)-\widetilde{R}_m(i)\right| \times\left|S\left(L-(m-L_s)\,s+i\right)-\widetilde{S}_m(i)\right|; \quad m = L_s+1,\cdots,2L_s \tag{4}$$

Here, $\widetilde{R}_m(i)$ and $\widetilde{S}_m(i)$ are the fitting polynomial in the segment m.

- Step 4: By averaging over all segments, the q^{th} order fluctuation function $F_q(s)$ can be determined as follows,

$$F_q(s) = \left[\frac{1}{2L_s}\sum_{m=1}^{2L_s}\left(F^2(s,m)\right)^{\frac{q}{2}}\right]^{\frac{1}{q}}; \quad q \neq 0 \tag{5}$$

Whereas, if $q \to 0$ the L'Hospital rule is used to determine the fluctuation function as follows,

$$F_0(s) = \exp\left[\frac{1}{4L_s}\sum_{m=1}^{2L_s}\ln\left|F^2(s,m)\right|\right] \tag{6}$$

- Step 5: In this final step, we determine the slope of the of $F_q(s)$ versus s plot from where the scalingexponent $h_{rs}(q)$ can be determined as:

$$F_q(s) \approx s^{h_{rs}(q)} \tag{7}$$

2.2 | Multifractal detrending moving average cross-correlation analysis (MFXDMA)

MFXDMA, like MFXDFA, entails all five of the preceding steps. Only step 3 distinguishes MFXDMA from MFXDFA. In contrast to MFXDFA, where $\widetilde{R}_m(i)$ and $\widetilde{S}_m(i)$ are fitting polynomials, $\widetilde{R}_m(i)$ and $\widetilde{S}_m(i)$ in MFXDMA are moving average functions in a moving window which can be mathematically expressed as (Zhou et al. 2011):

$$\widetilde{R}_m(i) = \frac{1}{l}\sum_{k=-\lfloor(l-1)\theta\rfloor}^{\lceil(l-1)(1-\theta)\rceil}\widetilde{R}_m(i-k); i = 1,2,\ \ldots\ ,L \tag{8}$$

where l and θ denote the sliding window and position parameter respectively. The parameter θ lies between 0 to 1. $\lfloor\alpha\rfloor$ is the greatest integer less than α, whereas $\lceil\alpha\rceil$ is the lowest integer greater than α. DMA analysis can be divided into three unique scenarios depending on the values of θ as: (i) $\theta = 1$, where all future $(l-1)$ data values are considered to compute the moving average function $\widetilde{R}_m(i)$. This unique condition is referred to as the forward-moving average. (ii) $\theta = 0$, $\widetilde{R}_m(i)$ is determined by considering all past $(l-1)$ data values of the signal, referred as the backward-moving average. (iii) $\theta = 0.5$, when the $\widetilde{R}_m(i)$ can be assessed using half past and half future data values of the time series, referred to as the centered moving average technique.

2.3 | Multifractal parameters

Here, we determined the Hurst exponent $h_{rs}(q)$, the scaling exponents $\tau_{rs}(q)$, which measures the multifractality of the cross-correlation of the cross-correlated time series. To analyze the singularities, we calculated the singularity strength $\alpha_{rs}(q)$ and also obtained the singularity spectrum $f_{rs}(\alpha)$.

The cross-correlation behavior between two signals depends on the relationship between $h_{rs}(q)$ and q. If $h_{rs}(q)$ is dependent on q then the behavior of cross-correlations between the two signals are multifractal otherwise monofractal. The specific value of $h_{rs}(2)$ is known as bivariate cross-correlation Hurst exponent. If the value of $h_{rs}(2)$ is less than 0.5 then it can be conclude that signals are cross anti-persistent or long-range anti-correlated whereas if the value is greater than 0.5 then the signals are cross persistent or long range correlated. The cross-correlations between two signals are entirely missing when the value of $h_{rs}(2)$ is equal to 0 or it can be said that for $h_{rs}(2) = 0$, short-range cross-correlations present between signals.

The scaling exponents $\tau_{rs}(q)$ can be determined from the relation between Hurst exponents and scaling exponents, given as

$$\tau_{rs}(q) = qh_{rs}(q) - 1 \tag{9}$$

Equation (13) can be modified as

$$\tau_{rs}(q) = qh_{rs}(q) - qh_{rs}(1) - 1 \tag{10}$$

If $\tau_{rs}(q)$ is varying non-linearly with q, then the behavior of cross-correlation is multifractal. The Singularity spectrum can be obtained by using Legendre transformation, given as

$$f_{rs}(\alpha) = q\alpha_{rs} - \tau_{rs}(q) \tag{11}$$

The width of the singularity spectrum reveals the degree of cross-multifractality.

Here, the parameter α is known as Lipschitz–Hölder exponent, which is computed from the slope of $\tau_{rs}(q)$ vs. q curve.

$$\alpha_{rs}(q) = \frac{d}{dq}\tau_{rs}(q) \tag{12}$$

3 | RESULT AND ANALYSIS

In Figure 3, the dependency of the $F(q)$, $h(q)$, $\tau(q)$ on q, the behavior of $\log(F\,[s])$ versus $\log(s)$ plot and the nature of the singularity spectrum $f(\alpha)$ are presented for both CME linear speed and Kp-index signals using MFXDFA algorithm. Also, the variation of the $(h_{rr} + h_{ss})/2$ along with q has been shown in Figure 3c. Here, the range of exponent q is taken as -10 to $+10$ with a fixed step interval 0.5 and the scale s in the range 10 to $(\leq L/5)$ (Kantelhardt et al. 2002).

The cross-correlation of the two time series signals has also been investigated by applying backward moving average-based MFXDMA ($\theta = 0$). Gu and Zhou demonstrated in their study (Gu and Zhou 2010) that among the three MFDMA approaches based on forward ($\theta = 1$), centered ($\theta = 0.5$), and backward ($\theta = 0$) moving average, the last one outperforms the other two. Singularity spectrum $f(\alpha)$ and $F(q)$, $h(q)$, $\tau(q)$ for both time series applying MFXDMA ($\theta = 0$) are shown in Figure 4. Here, the parameter s varied from 10 to L/10 (Gu and Zhou 2010) and q is set in steps of 0.5 from -10 to $+10$.

The nonlinear nature of $F(q)$ function can be noticed in Figure 3a which advocates for the multifractal characteristics of both signals. The multifractal character is further supported by a similar fluctuation in the slope of the $F(q)$ with q as shown in Figure 4a. It can be seen in Figure 3b that the values of $\log(F\,(s))$ increases as $\log(s)$ increases which confirms the presence of a power-law cross-correlation between CME and Kp-index. In Figure 3c, the decreasing relationship between $h(q)$ and q has been observed. This nature of the $h(q)$ function reveals that the small fluctuation scaling properties are more dominant compared to the large fluctuation scaling properties for both signals (Ausloos 2012). Also, the cross-correlation Hurst exponent has been determined from Figure 3c, which is 0.79341 ± 0.028982. It is found that the value of $h_{rs}(2)$ is greater than 0.5, which confirms the presence of positive persistence temperament in the cross-correlations.

The $h(q)$ is computed for MFXDMA ($\theta = 0$) and presented in Figure 4b for various q values. The $h(q)$, like the MFDFA, is shown to have a nonlinear dependence on q. The backward MFXDMA analysis verifies MFXDFA's claim that both time series data are not mono-fractal but have multifractal properties because mono-fractal time series has a constant $h(q)$ value (Kantelhardt et al. 2002). The reduction in values of the $h(q)$ with q implies that the scaling qualities of minor fluctuations of the data are higher than the big fluctuations, which is the same point made by the MFXDFA analysis. The computed value of the cross-correlation Hurst exponent $h_{rs}(2) = 1.0644 \pm 0.020328$ validates a significant positive long-term memory in the cross-correlations between the two time series. The non-stationary nature of the signals is further supported by the unity value of $h_{rs}(2)$. For each q, the values of the $\tau_{rs}(q)$ are computed using Equation (10) and plotted in Figures 3d and 4c for MFXDFA and MFXDMA ($\theta = 0$) respectively. In Figure 3d and 4c, the $\tau_{rs}(q)$ function exhibits nonlinear nature with respect to q, which

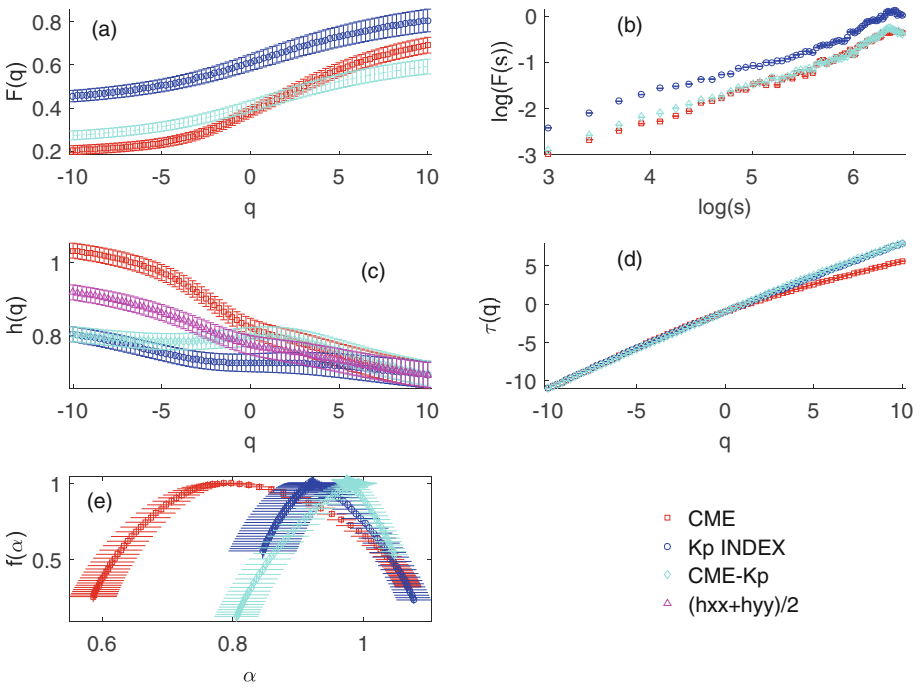

FIGURE 3 MFXDFA plots for CME linear speed and Kp-index (a) $F(q)$ versus q (b) $\log(F\,(s))$ versus $\log(s)$ (c) $h(q)$ versus q (d) $\tau(q)$ versus q (e) $f(\alpha)$ versus α

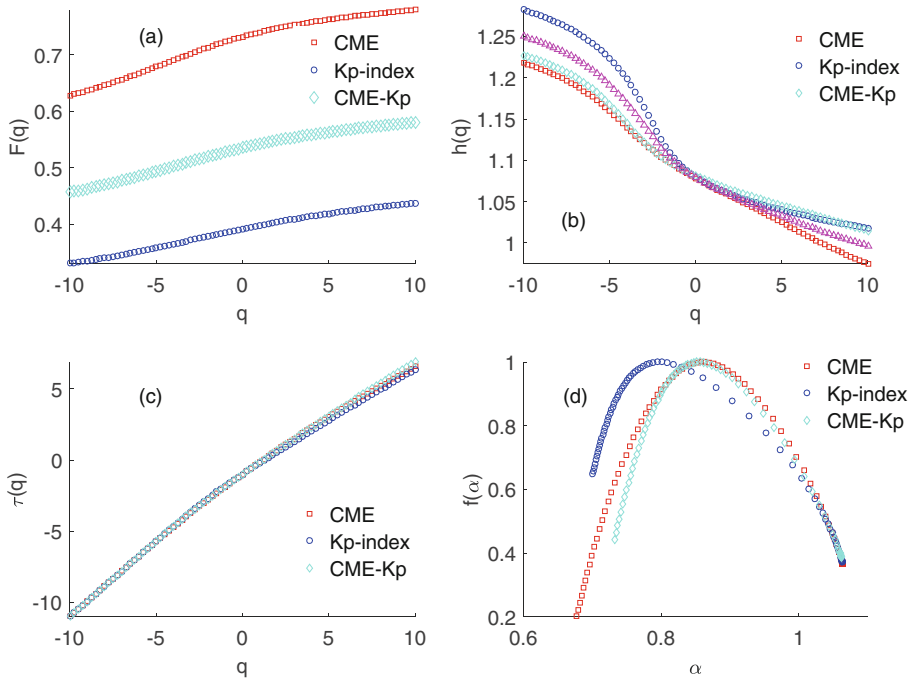

FIGURE 4 MFXDMA ($\theta = 0$) plots for CME linear speed and Kp-index (a) $F(q)$ versus q (b) $h(q)$ versus q (c) $\tau(q)$ versus q (d) $f(\alpha)$ versus α

reveals the possibility of multiple scaling in corresponding cross-correlations, while the degree of multifractality indicates by the degree of nonlinearity of the $\tau(q)$ function.

The singularity spectrum $f(\alpha)$ of MFXDFA and MFXDMA has been portrayed in Figure 3e and 4d respectively. The singularity spectrum is one of the essential functions used to emphasize multifractal behavior (Shimizu et al. 2002). The degree of multifractality of a signal can be measured by computing the width of the singularity spectrum. The broad singularity width suggests that the cross-correlations between the two time series exhibit multifractal behavior. The critical parameters $\alpha_{\min}, \alpha_{\max}, \Delta\alpha, \alpha_0$ for both data series are obtained and reported in Table 1 by extrapolating the singularity spectrum.

The maximum and minimum singularity strengths are denoted as $\alpha_{\min}$ and $\alpha_{\max}$, respectively, while these two parameters are the lowest and highest values of the Hölder exponent α of the spectrum for which $f(\alpha) = 0$. In this work, the computed values of $\alpha_{rs\min}$ and $\alpha_{rs\max}$ for cross-correlation analysis using MFXDFA are 0.8055 and 1.0468, respectively, whereas for MFXDMA $\alpha_{rs\min}$ and $\alpha_{rs\min}$ are 0.7322 and 1.0614, respectively. The spectrum width can be defined as the difference between the $\alpha_{rs\min}$ and $\alpha_{rs\min}$ (denoted as $\Delta\alpha_{rs}$), which measures the length of the range of fractal exponents in the signal, that is, the degree of multifractality. Here, the computed values of the $\Delta\alpha_{rs}$ for MFXDFA and MFXDMA ($\theta = 0$) are 0.2413 and 0.3292 respectively.

The shape of the singularity spectrum depends upon the parameter δ, which can be obtained by fitting the spectrum to a quadratic equation around α_0, that is, $f(\alpha) = \delta(\alpha - \alpha_0)^2 + \gamma(\alpha - \alpha_0) + f_{\max}$ (Dutta et al. 2013). The polarity of δ determines the direction in which the parabolic shape of the spectrum opens up; positive δ produces a U-shaped parabola, whereas negative δ produces an inverted U-shaped parabola. The degree of openness of the parabola is inversely proportional to δ's magnitude, that is, the value of δ is inversely related to spectrum width ($\Delta\alpha$). A larger δ will compress the spectrum curve inward, whereas a lesser δ would extend it outward. It is evident from Figures 3e and 4d that δ is negative. The symmetry of the spectrum (right/left skewed/symmetric) determines whether high (or low) fluctuations predominate. It can be quantified by a measure known as the Asymmetry Index (AI) which is determined using the width of the parabola's right and left wings as follows: $AI = \Delta\alpha_{left} - \Delta\alpha_{right}/\Delta\alpha_{left} + \Delta\alpha_{right}$. Here, $\Delta\alpha_{right}$ and $\Delta\alpha_{left}$ can be determined as $\alpha_{rs\max} - \alpha_{rs_0}$ and $\alpha_{rs_0} - \alpha_{rs\min}$ respectively. The zero value of AI indicates that the spectrum is symmetric, while the negative and positive magnitudes suggest a left-skewed or right-skewed spectrum. A negative AI value indicates that the multifractality is unaffected by small-magnitude local fluctuations, implying that extreme occurrences occur frequently. Here, the computed AI values for both MFXDFA and MFXDMA ($\theta = 0$) analysis are negative magnitudes as shown in Table 1.

In Figure 5, the outcomes of the MFXDFA and MFXDMA ($\theta = 0$) algorithms have been compared.

TABLE 1 Cross-correlation parameters of CME and Kp-index using MFXDFA and MFXDMA

Cross-correlation	$\alpha_{rs\,\min}(f=0)$	$\alpha_{rs\,\max}(f=0)$	$\Delta\alpha_{rs}\left(\alpha_{rs\,\max}-\alpha_{rs\,\min}\right)$	$h_{rs}(q=2)$	α_{rs_0}	$AI=\frac{\Delta\alpha_{left}-\Delta\alpha_{right}}{\Delta\alpha_{left}+\Delta\alpha_{right}}$
$MFXDFA_{CME\text{-}Kp}$	0.8055	1.0468	0.2413	0.79+/− 0.02	0.9735	−0.1950
$MFXDMA_{CME\text{-}Kp}$	0.7322	1.0614	0.3292	1.06+/− 0.02	0.8567	−0.2436

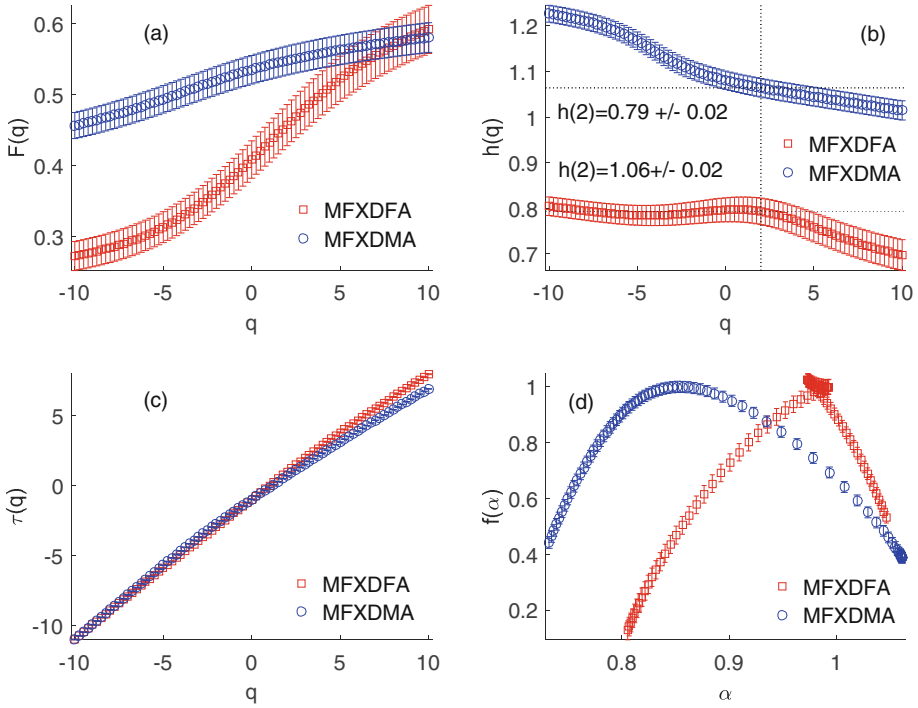

FIGURE 5 Comparative study of the plots using MFXDFA and backward MFXDMA for (a) $F(q)$ versus q (b) $h(q)$ versus q(c) $\tau(q)$ versus q (d) $f(\alpha)$ versus α

It is evident from Figure 5a–d that in comparison to the MFXDFA, the backward MFXDMA more precisely reveals cross-correlations between the two time series exhibiting multifractal behavior. The computed degree of multifractality ($\Delta\alpha_{rs}$) for cross-correlation analysis applying backward MFXDMA is greater than that of MFXDFA, as shown in Table 1 and Figure 5d. The comparative analysis uncovers some interesting points:

i. The rise of the $F(q)$ is greater for MFXDMA ($\theta=0$) than for MFXDFA.
ii. The $h_{rs}(2)$ value obtained using the MFXDMA ($\theta=0$) technique is greater than the MFXDFA method.
iii. The degree of nonlinearity of $\tau_{rs}(q)$ in backward MFXDMA and MFXDFA is approximately the same.
iv. MFXDMA ($\theta=0$) has a broader singularity spectrum than MFXDFA.
v. The uncertainty (indicated by the error bar) associated with the cross-correlation Hurst exponent is essentially the same for the MFXDFA and backward MFDMA methods.

Therefore, it can be noted that the backward MFXDMA approach is more apparent than the MFXDFA method in terms of cross-correlation analysis of the CME linear speed and Kp-index time series signals.

4 | CONCLUSION

i. The CME and Kp-index, along with their cross-correlation, exhibit power law behavior.
ii. The Hurst exponent $h_{rs}(2)$ of the cross-correlation generated by the MFXDMA ($\theta=0$) and MFXDFA algorithms is more than 0.5, suggesting that the cross-correlations between the time series under investigation have strong positive long-term memory.
iii. The scaling exponent reveals the possibility of multiple scaling in corresponding cross-correlations.
iv. The width of the singularity spectrum suggests that the range of the fractal exponents existing in the cross-correlation is quite significant.
v. The negative values of AI for both MFXDFA and MFXDMA ($\theta=0$) advocate for the occurrence of severe events on a regular basis.

vi. The different computed cross-correlation parameters validate the better performance of backward MFXDMA over the MFXDFA.
vii. The CME linear speed and Kp-index signals have self-similar patterns. Furthermore, the structural patterns of CME linear speed are significantly correlated with the Kp-index signal with a long-range correlation.

ORCID

Anirban Chattopadhyay https://orcid.org/0000-0002-1216-0533

REFERENCES

Ausloos, M. 2012, *Phys. Rev. E*, *86*(3), 1.
Chattopadhyay, A., Khondekar, M. H., & Bhattacharjee, A. K. 2017, *Astrophys. Space Sci.*, *362*(9), 179.
Chattopadhyay, A., Khondekar, M. H., & Bhattacharjee, A. K. 2018, *Chaos Solit. Fractals.*, *114*, 542.
Cooper, G. R. J., & Cowan, D. R. 2008, *Comput. Geosci.*, *34*(2), 95.
Dutta, S., Ghosh, D., & Chatterjee, S. 2013, *Front. Physiol.*, *4*, 274.
Echer, E., Gonzalez, W. D., & Alves, M. V. 2006, *Space Weather*, *4*(6), S06001.
Gopalswamy, N. 2009, *J. Geophys. Res. Space Phys.*, *114*(A3), 1.
Gopalswamy, N., Yashiro, S., Michalek, G., Stenborg, G., Vourlidas, A., Freeland, S., & Howard, R. 2009, *Earth Moon Planets*, *104*(1), 295.
Gu, G. F., & Zhou, W. X. 2010, *Phys. Rev. E*, *82*(1), 011136.
Hapgood, M. 2012, *Nature*, *484*(7394), 311.
Holappa, L., Mursula, K., Asikainen, T., & Richardson, I. G. 2014, *J. Geophys. Res. Space Phys.*, *119*(6), 4544.
Horvath, I., & Lovell, B. C. 2017, *Space Phys.*, *122*(11), 765.
Huttunen, K. E. J., Kilpua, S. P., Pulkkinen, A., Viljanen, A., & Tanskanen, E. 2008, *Space Weather*, *6*(10), 1. https://doi.org/10.1029/2007SW000374.
Jordanova, V. K., Albert, J., & Miyoshi, Y. 2008, *J. Geophys. Res. Space Phys.*, *113*(A3), 1. https://doi.org/10.1029/2008JA013239.
Kantelhardt, J. W., Zschiegner, S. A., Koscielny-Bunde, E., Havlin, S., Bunde, A., & Stanley, H. E. 2002, *Physica A*, *316*(1), 87.
Kappenman, J. G. 1996, *IEEE Power Eng. Rev.*, *16*(5), 5.
Kappenman, J. G. 2012, *IEEE Spectrum*, *49*(2), 26.
Keesee, A. M., Scime, E., & Moldwin, M. B. 2008, *J. Geophys. Res. Space Phys.*, *113*(A3), 1. https://doi.org/10.1029/2008JA013130.
Mansilla, G. A. 2013, *Atmos. Clim. Sci.*, *3*, 475.
Menvielle, M., & Berthelier, A. 1991, *Rev. Geophys.*, *29*(3), 415.
Ni, Y. Y. 2017, *IOP Conf. Ser.: Mater. Scie. Eng.*, *339*(1), 1. https://doi.org/10.1088/1757-899X/339/1/012013.
Papaioannou, A., Mavromichalaki, H., Eroshenko, E., Belov, A., & Oleneva, V. 2009, *Ann. Geophys*, *27*, 1019.
Sahai, Y. D., Jesus, R., Fagundes, P. R., et al. 2012, *Adv. Space Res.*, *50*(10), 1344.
Shimizu, Y., Thurner, S., & Ehrenberger, K. 2002, *Fractals*, *10*(1), 103.
Suvorova, A. V., Huang, C. M., Tsai, L. C., Dmitriev, A. V., & Ratovsky, K. G. 2015, *Adv. Space Res.*, *56*(9), 2001.
Thomson, A. W., Gaunt, C. T., Cilliers, P., et al. 2010, *Adv. Space Res.*, *45*(9), 1182.
Villante, U., & Regi, M. 2008, *J. Geophys. Res. Space Phys.*, *113*(A3), 1.
Zhao, B., Wan, W., Tschu, K., et al. 2008, *J. Geophys. Res. Space Phys.*, *113*(A3), 1.
Zhou, W. X. 2008, *Phys. Rev. E*, *77*(6), 066211.
Zhou, Y., Leung, Y., & Yu, Z. G. 2011, *Chin. Phys. B*, *20*(9), 090507.

AUTHOR BIOGRAPHY

Anirban Chattopadhyay is a Ph.D. student at the Electronics & Communication engineering (ECE) Department, National Institute of Technology (NIT) Durgapur. He is working as an Assistant Professor in the ECE Department of Dr. B.C. Roy College of Engineering, Durgapur. His research interests include Time Series Analysis, Astrophysical Signal analysis. He is actively involved in research and producing high quality research work. He has published four articles in SCI journals.

How to cite this article: Chattopadhyay, A., & Khondekar, M. H. 2023, *Astron. Nachr.*, e20220042. https://doi.org/10.1002/asna.20220042